A New Model for Quantifying the Extent of Interaction between Soluble Polyphenylene-Vinylenes and Single-Walled Carbon Nanotubes in Solvent Dispersions

ARTICLE *in* THE JOURNAL OF PHYSICAL CHEMISTRY B · SEPTEMBER 2010

Impact Factor: 3.3 · DOI: 10.1021/jp104705y · Source: PubMed

A New Model for Quantifying the Extent of Interaction between Soluble Polyphenylene-Vinylenes and Single-Walled Carbon Nanotubes in Solvent Dispersions

Christopher J. Collison,* Susan Spencer, Amanda Preske, Chad Palumbo, Alysha Helenic, Rebecca Bailey, and Steven Pellizzeri

Department of Chemistry, College of Science, Rochester Institute of Technology, 84 Lomb Memorial Drive, Rochester, New York 14623-5603

Received: May 21, 2010; Revised Manuscript Received: July 19, 2010

The ability to disperse and, hence, manipulate single-walled carbon nanotubes is critical for their use in organic photovoltaic devices, either as a transparent electrode or as an electron acceptor material. We present data to quantify the physical interaction of single wall carbon nanotubes (SWCNTs) with two soluble phenylene vinylene conjugated polymers, poly[2′-methoxy-5-(2′-ethylhexyloxy)-1,4-phenylenevinylene] and poly(2,5-di(hexyloxy)cyanoterephthalylidene). We provide static quenching constants, associated with polymer-SWCNT complexation, as a weight percent ratio of polymer to nanotubes for different solvent and polymer concentration conditions. Optimization of conditions for nanotube dispersion using a given polymer can now be predicted, and furthermore, we can describe a technique allowing for enhanced relative comparisons of polymer materials for nanotube dispersion.

Introduction

Organic photovoltaic devices offer the potential of flexible, low-cost options for future renewable energy that will reduce humanity's reliance on oil and other fossil fuels. Single-wall carbon nanotubes (SWCNTs) provide possibilities[1−9] for improving the efficiency of photovoltaic devices through increasing the conductivity of composite materials, as a charge acceptor in a bulk heterojunction device or as a replacement for indium tin oxide (ITO) as the transparent electrode. Films and composites processed from SWCNTs that are well dispersed in solvent offer an enormous potential for novel conductive fibers, papers, flexible films, and even reel-to-reel processed photovoltaic devices[10] because of the SWCNTs' inherent flexibility. Our broad goal is to improve the fundamental understanding of physiochemical interactions between conducting polymers and SWCNTs, two important components of organic photovoltaic devices. The physical interaction of the SWCNTs and polymers, in general, is critical for better processing and deposition of carbon nanotubes, given their low dispersion limit in a range of solvents. Furthermore, once the type and morphology of the physical interaction is described in detail, we can identify the energy transfer and charge transfer components of fluorescence quenching of the polymers by the SWCNTs.

A substantial volume of work involving organic photovoltaic devices (OPVs) made of poly[2-methoxy-5-(2′-ethyl-hexyloxy)-1,4-phenylene vinylene] (MEH-PPV) and functionalized C_{60} fullerenes exists.[11] However, relatively little work has been done to investigate charge transfer in OPVs from MEH-PPV to *carbon nanotubes*, which offer distinct advantages through their extremely high aspect ratios and high electron mobility.[12,13] This is understandable, however, given that SWCNTs provide unique difficulties in production, dispersion, and characterization because they are nonreactive and have low dispersion limits in solution.[14]

Work continues to better understand the interaction of SWCNTs with small molecules and solvents such that processing of SWCNTs might be improved.[15] However, a strong understanding at the molecular level of polymer-SWCNT interfaces is lacking. Despite the experimental challenges presented, there is clear potential for SWCNTs to be a very powerful contributor to increased efficiency of organic photovoltaic devices.

SWCNTs can be synthesized in different ways, with each synthesis approach resulting in a unique mixture of diameter and chirality.[16] Yet any synthesized mixture includes both semiconducting and metallic nanotubes. As a result, nanotube mixtures act as ubiquitous fluorescence quenchers when added to a luminescent sample in solution. The extent of quenching will depend upon the relative amount of metallic tubes, the proportion of semiconducting tubes having electronic states aligned appropriately with the fluorophore excited state, and the extent of nanotube debundling. The LUMO energy level of the semiconducting nanotubes and the Fermi energy level of the metallic nanotubes is understood to be in a range 4.5−5.0 eV below the vacuum level.[17] Ideally, therefore, the LUMO energy level of the fluorophore or conjugated polymer must be greater (higher than −4.5 eV relative to vacuum) than that of the SWCNT. Bandgap discussions are inherently generalized, however; of greater importance is that quenching is particularly sensitive to the degree of complexation of the nanotubes with the fluorophore, especially in solution.

An overarching theme is that fluorescence quenching studies allow us to better understand what functional groups, on a variety of dispersants or surfactants, lead to stronger complexation of the nanotubes. Hence, systematic variations in dispersant molecules can provide guidance as to how nanotube dispersion and manipulation can be improved. Fluorescence quenching studies also allow us to compare interactions between small molecules and nanotubes with interactions between conjugated polymers and SWCNTs so as to appreciate the role of molecular weight in the improved dispersion of SWCNTs. Furthermore.

* Corresponding author. E-mail: cjcscha@rit.edu.

10.1021/jp104705y
Published on Web 08/10/2010

a study of the effect of rigidity and conformation on complexation with SWCNTs can also be addressed.

Collison et al. have already demonstrated that complexation between nanotubes and MEH-PPV or poly(2,5-di(hexyloxy)cyanoterephthalylidene) (CN-PPV) is likely, given the appropriate solvent conditions.[18] In this work, we present the results of fluorescence quenching measurements performed under a variety of conditions for the two fluorophores MEH-PPV and CN-PPV to generate a significant volume of data so that the quenching mechanism can be determined. Support for this complexation and a further assessment of the electronic interaction can be achieved by studying the energy transfer and fluorescence quenching in depth, which allows us to propose a model for energy transfer that is tested using Stern−Volmer type fluorescence quenching experiments. Our model supposes two mechanisms for quenching: (1) immediate quenching of fluorophores adjacent to a nanotube within polymer-SWCNT complexes and (2) dynamic quenching of a fluorophore that is free in solution.

Lakowicz[19] provides a Stern−Volmer equation derivation that addresses both quenching mechanisms; when they are both occurring simultaneously, they combine to give a quadratic curve in the Stern−Volmer plot. However, we soon found that this preexisting model for evaluating fluorescence quenching data could not be applied to the systems with large polymer fluorophores (MEH-PPV, CN-PPV) and SWCNTs. These systems demonstrated significant sigmoidal curvature in the Stern−Volmer plot. Furthermore, both MEH-PPV and CN-PPV generated differing quenching constants, depending on the concentration of the polymer, an unexpected result. Therefore, a new Stern−Volmer equation is derived, and the model is tested whereby the curvature can be quantified and understood in terms of the polymer-SWCNT physical interaction. This new model allows for an analysis that is both descriptive and quantifiable; the modified Stern−Volmer equation used has been applied to all data generated in this work and serves as both a predictive description of how the polymers will spatially interact with the SWCNTs as well as an explanatory model of the physiochemical transitions occurring between quencher and fluorophore.

As a control, we further demonstrate conventional linear Stern−Volmer quenching of (i) MEH-PPV by a SWCNT single molecule analog, [6,6]-phenyl-C61-butyric acid methyl ester (PCBM), and (ii) a small molecule analog of MEH-PPV, 1,4-bis[(2−92-methylphenyl)ethenyl]-benzene (BMSB) by SWCNT.

Our proposed mechanism accounts for both complex formation via static quenching as well as dynamic quenching via collisions through diffusional interactions of the two species in solution.

We use this data combined with our new model as further support for complexation between SWCNTs and polymers, and we discuss the importance of further investigation to understand better the electronic interactions of conjugated polymers and SWCNTs. The ability to quantify fluorescence quenching offers far-reaching benefits because we can then begin to describe energy transfer to single sets of nanotubes on the basis of (1) the extent of physiochemical direct interaction of polymer and SWCNT and (2) the diffusional interactions of SWNCT, polymer, and solvent. We can also start to predict the optimal concentrations of polymer that can be used for stabilizing suspensions of SWCNT for processing so as to minimize the overuse of materials acting as surfactants.

Experimental Methods

Materials. The polyphenylenevinylene derivative MEH-PPV (CAS 138184-36-8, average M_n 40 000−70 000 and polydispersity 6) was purchased from Sigma-Aldrich. *N*,*N*-dimethylethanamide (DMA) (99% Spectrophotometric grade) solvent was purchased from Sigma-Aldrich. BMSB (CAS 13280-61-0, 99.5+%) was purchased from Sigma-Aldrich. PCBM was purchased from American Dye Source, Inc. with a purity of >99.5%. 1,2-Dichlorobenzene (ReagentPlus 99%) (DCB) was purchased from Sigma-Aldrich.

Dry S-P95-03-grade CoMoCat single-wall carbon nanotubes were purchased from Southwest Nanotechnologies Inc., with a quality factor of 0.94 and average tube length of 1 μm. All chemicals were used without further purification. Nanotubes were used as received.

Nanotube−Polymer Solution Preparation. Stock solutions of MEH-PPV were made by adding solvent to dry solid and by subsequent agitation with a Thermolyne Type 16700 mixer. Stable stock solutions of SWCNTs were made up using a similar approach to Landi et al.[14] using an ultrasonic bath (VWR, model 75D Ultrasonic Cleaner, 38.5−40.5 kHz) for 30 min of sonication time at its maximum power setting (90 W average power, 180 W peak power). We have empirically determined in separate experiments that nanotube dispersion is particularly sensitive to sonication time, so it was important to retain a fixed standard procedure for making up solutions. Mixing was optimized in composite solutions by adding the required volume of stock SWCNT solution to a sample vial containing an appropriate MEH-PPV solution. UV−vis data were recorded on all solutions such that the final SWCNT concentrations could be monitored in terms of OD, despite the difficulties of accurately achieving target concentrations because of the inherent heterogeneity of SWCNT stock solutions. DMA composite solutions were sonicated for 2 min prior to absorbance/fluorescence measurement. DCB composite solutions were shaken vigorously for 1 min because we recognize that sonication has an effect on the photophysics of MEH-PPV in this particular solvent. On the other hand, experiments in our lab show that extensive bath sonication of MEH-PPV in DMA has a minimal effect on the photophysics of the MEH-PPV sample.

Spectroscopic Methods. UV−vis absorption spectra were recorded with a Shimadzu high-resolution UV2401 UV−vis spectrophotometer and with a Perkin-Elmer Lambda 900 UV−vis−NIR spectrophotometer (SWCNT characterization). Fluorescence spectra were collected with a Perkin-Elmer LS-55 using a front surface accessory that compensates for inner filter effects[20] in more concentrated solutions by imaging the volume of solution at the front surface of the cuvette. All spectra were recorded using 1 cm quartz cuvettes from Starna Cells. Error bars shown in individual Stern−Volmer plots below represent the percentage error and are calculated from the standard deviation of the area under the fluorescence curve divided by the average of the area under the measured fluorescence. The average and standard deviation are calculated for five repeated measurements using the same sample and are representative of the instrumental uncertainty.

Spectroscopic Fitting. Absorbance of polymer/SWCNT composite solutions was reconstructed over the full range (300−800 nm) with a combination of, respectively, pure polymer in DMA and pure as-received CoMoCat SWCNT in DMA of targeted concentration. In other words, the measured absorbance of a composite dispersion of 0.142 OD MEH-PPV and 7 μg/mL of SWCNT was reconstructed from spectra of 0.142 OD MEH-PPV in DMA and of pure, as-received CoMoCat SWCNT, of concentration 7 μg/mL. The reconstruction was best fit to the measured data over the full spectral range.

The measured spectra were hence corrected for SWCNT absorbance by subtracting the SWCNT absorbance contribution, (the coefficients of best fit for the constructed spectra (0.98 ± 0.03 at 95% confidence) for SWCNT absorbance multiplied by actual SWCNT absorbance of the reference dispersion). This would leave a representation of the polymer absorbance in that composite dispersion. We also present the difference between raw absorbance data and constructed spectra.

Model Fitting. Fluorescence intensity for each solution in a SWCNT dilution series was measured with the same instrumental parameters. Fluorescence was excited at 450 nm, and the averaged intensity over the range 500−700 nm was consistently used for the Stern−Volmer plots. Stern−Volmer graphs were plotted as a function of nanotube absorbance at 700 nm; thus, at a region of no absorbance for the polymer. It is more instructive in this work to plot Stern−Volmer graphs as a function of solution absorbance. This is because targeted concentrations for SWCNTs are rarely achieved because of difficulties in overcoming errors in microbalance measurements, differing dispersion stabilities, etc. The model provided below was then fit to the data and parameters for the static quenching constant, and dynamic quenching constant was extracted. R^2 values for the fit were calculated. The average R^2 value for all 23 dilution series is 0.980, with a standard deviation of 0.023. Error bars are calculated based on three-fold replications of two dilution series for MEH-PPV and CN-PPV in DCB with targeted polymer concentrations of 1.0 and 2.5 μg/mL, respectively. In each case, the standard deviation of the fitted quenching constants K_{static} and $K_{dynamic}$ is calculated and divided by the average, to obtain a percentage error that is applied to the plotted data. The percentage errors for MEH-PPV (34% and 17%, respectively, in K_{static} and $K_{dynamic}$) are applied to all MEH-PPV data points, and the percentage error for CN-PPV (73% and 2% respectively in K_{static} and $K_{dynamic}$) are applied to all CN-PPV data points to give the error bars. The increased curvature of the MEH-PPV Stern−Volmer plots results in a tighter reproducibility in the static quenching constant, whereas the greater contribution of dynamic quenching constant (and lower curvature) for CN-PPV Stern−Volmer plots results in a smaller error in the dynamic quenching constant and a larger error in static quenching constant. These are demonstrated in the error bars of Figures 9−12.

Results and Discussion

The fluorescence and absorption spectra of MEH-PPV and CN-PPV in DMA solution are shown in Figure 1. The absorption spectrum of a 5 μg/mL CoMoCat SWCNT dispersion in DMA is shown in Figure 2.

We turn our attention first to the changes in the absorbance spectrum and fluorescence spectrum as SWCNTs are added to MEH-PPV in DMA solution. The changes in the absorbance spectrum are shown in Figure 3a−c. An increase in the absorbance spectrum beyond a simple sum of the pure MEH-PPV and SWCNT solution spectra is apparent at 570−580 nm. This is assigned to the complexation of MEH-PPV with SWCNT. This complexation is discussed qualitatively elsewhere[18] and quantitatively within this work.

The changes to the fluorescence spectra and the decreases in intensity are shown in Figure 4. The spectral shifts for MEH-PPV (Figure 4a) are associated with the predominant quenching of shorter conjugation length excited states given a broad distribution of conformers in a DMA solution. This result is also discussed in more detail elsewhere.[18] There is a very slight blue shift for CN-PPV solutions as SWCNT is added to solution

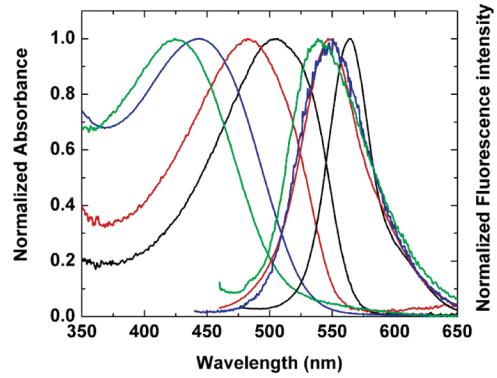

Figure 1. Normalized absorption and fluorescence emission spectra of MEH-PPV in DCB (black) and DMA (red) and of CN-PPV in DCB (blue) and DMA (green). All emission spectra were excited at 450 nm and were measured with front-face geometry, consistent with quenching experiments.

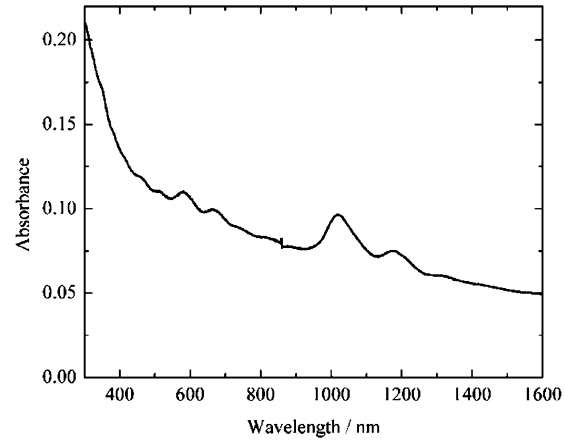

Figure 2. Absorbance of as-received CoMoCat single-walled nanotubes in DMA with a 5 μg/mL target concentration.

(Figure 4b). In this work, our emphasis is on describing the quenching in a more quantitative way. Consequently, a Stern−Volmer type plot is provided in Figure 5, which demonstrates the extent of quenching for the total fluorescence as measured for the range 500−700 nm. The Stern−Volmer plot has a characteristic curvature away from the x-axis at low concentrations of nanotubes. We also observe a plateau being reached at ~9 μg/mL of SWCNTs, which represents a point of maximum quenching for this polymer in solution with an optical density of 0.231 (corresponding to 9 μg/mL of MEH-PPV).

The dependence of polymer fluorescence intensity on the concentration of SWCNTs was initially modeled by using the Stern−Volmer equation, expressed as

$$\frac{I_0}{I} = 1 + K_{SV}[\text{SWCNT}] \quad (1)$$

where I_0 and I are the fluorescence intensities in the absence and presence of quencher, respectively, K_{SV} is the Stern−Volmer quenching constant, and [SWCNT] is the concentration of the SWCNT quencher. The quenching constant is typically obtained from the slope of a linear fit to a plot of I_0/I versus [SWCNT]. Through inspection, one can observe that a straight line fit will not be a good one and that the simplified Stern−Volmer model is inadequate for this system. However, deviations from the linear relationship are traditionally observed in certain situations outlined as follows: (i) when the quenching efficiencies are very

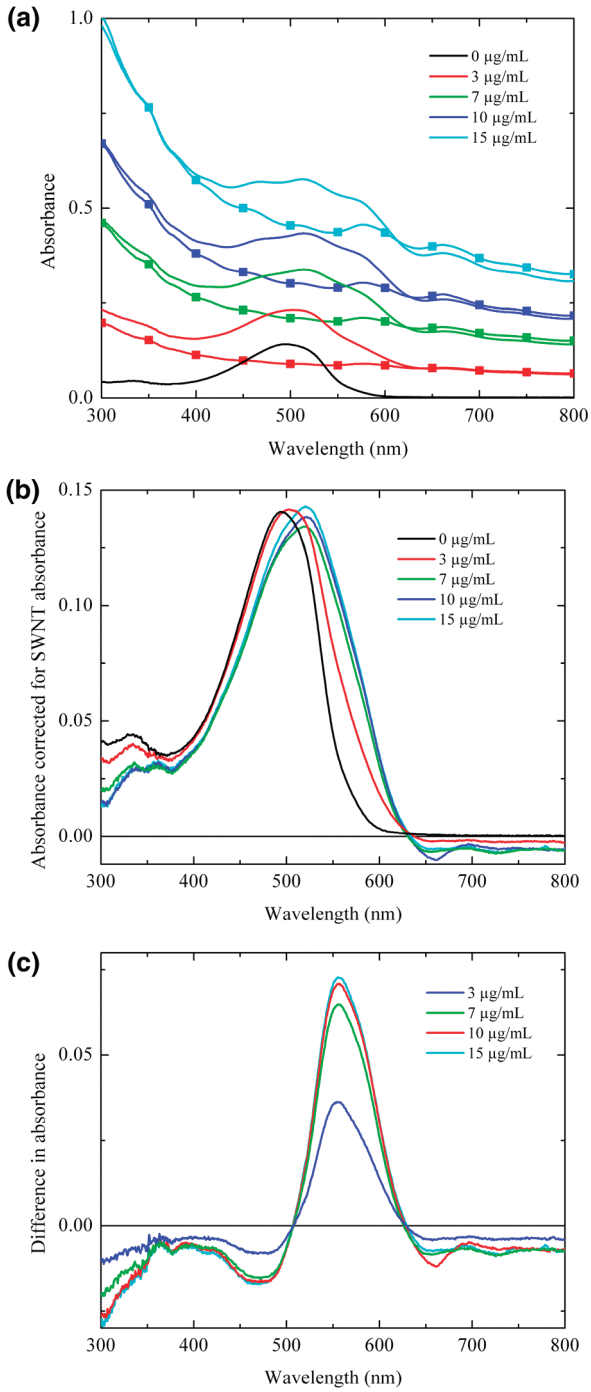

Figure 3. a. Raw absorbance data of 0.142 OD MEH-PPV in DMA as a function of SWCNT concentration. Lines with squares are the measured absorbance spectra of nanotube dispersions in DMA, of the appropriate concentration so as to directly compare with composite dispersions spectra. b. Absorbance of MEH-PPV corrected for SWCNT absorbance for dispersions of varying SWCNT concentration. c. For dispersions of varying SWCNT concentration, we present the difference between raw absorbance data and constructed spectra.

high, as observed in superquenching of conjugated polyelectrolytes by gold nanoparticles;[21] (ii) if two fluorophore populations are present and one class is not available to the quencher;[22] or (iii) if the fluorophore is being quenched both by collisions and by complex formation with the same quencher.[19]

With a classical straight line fit, the slope value of K_{SV} is typically associated with the specific mechanism of quenching: either diffusional quenching when it is a bimolecular rate constant or static quenching when it is an equilibrium constant.

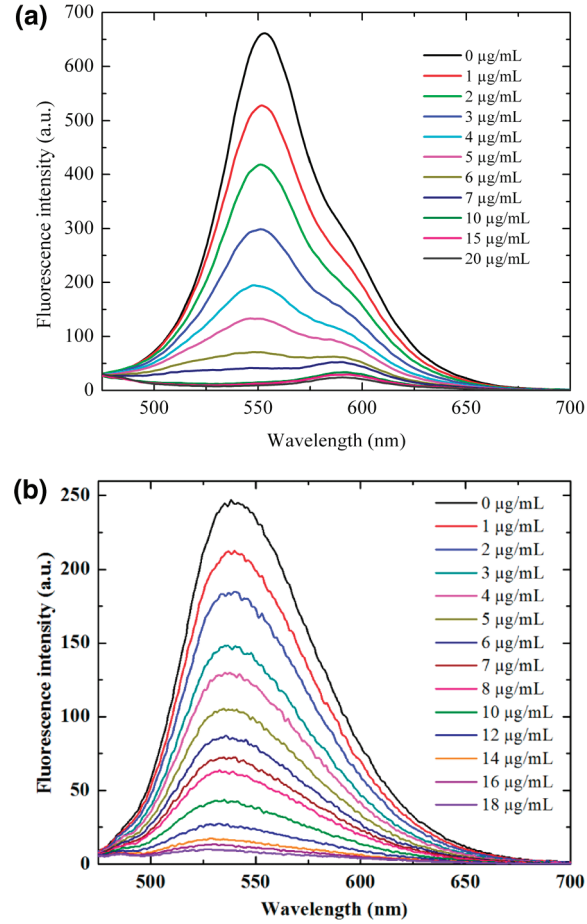

Figure 4. a. Fluorescence spectra of 9 μg/mL solutions of MEH-PPV as a function of added CoMoCat SWCNT concentration. The solvent is DMA, and the excitation wavelength is 450 nm. b. Fluorescence spectra of 4.7 μg/mL solutions of CN-PPV as a function of added CoMoCat SWCNT concentration. The solvent is DMA, and the excitation wavelength is 450 nm.

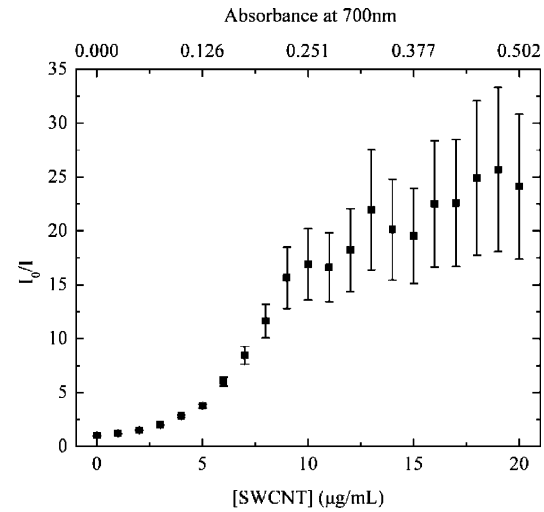

Figure 5. Stern−Volmer plot for 9 μg/mL MEH-PPV in DMA as a function of targeted SWCNT concentration in micrograms of SWCNT per milliliter (bottom axis) of solvent and optical density at 700 nm (top axis). Fluorescence excitation wavelength is 450 nm.

This equation generates a linear plot of the data presented here when the solutions under study contain either small molecules and SWCNTs or polymers and small molecule quenchers.

Linear Stern−Volmer plots from two control experiments are shown in Figures 6 and 7. First, MEH-PPV is quenched by

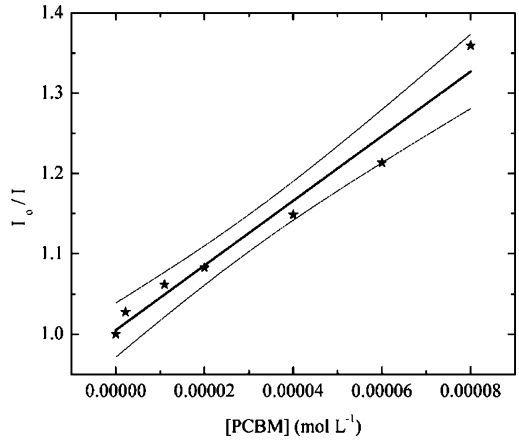

Figure 6. Stern−Volmer plot of MEH-PPV fluorescence quenching by PCBM in DMA. Faint gray lines show 95% confidence bands. Stern Volmer constant is 4027 ± 811 L/mol at 95% confidence limit.

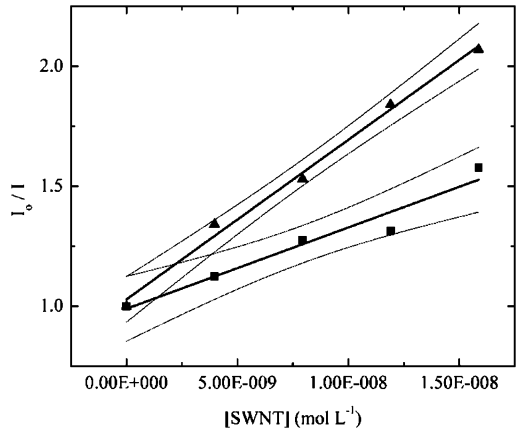

Figure 7. Stern−Volmer plot of BMSB fluorescence quenching by SWCNT in DCB at 20 °C (triangles) and at 70 °C (squares). Faint gray lines show 95% confidence bands. Stern Volmer constants are 6.65 ± 0.30 × 107 L/mol and 3.39 ± 0.44 × 107 L/mol (errors at 95% confidence limit, SWCNT molar mass estimated as 1.3 × 106 g/mol).

PCBM in DCB. The plot in Figure 6 is indicative of quenching by a diffusional mechanism (in accordance with the diffusional quenching invoked by Wang et al[23]). In Figure 7, we observe the fluorescence quenching of the MEH-PPV small molecule analog, 1,4-bis[2-(2-methylphenyl)ethenyl]-benzene (BMSB), quenched now by SWCNTs at room temperature (20 °C) and high temperature (70 °C). In this case, the temperature dependence suggests a static quenching mechanism, since complexing, and hence quenching, would decrease as temperature increased.

These two sets of data are in stark contrast to the data measured for quenching of MEH-PPV by SWCNTs in which nonlinear plots are always observed. As mentioned above, nonlinear plots are often observed when there is a combination of static and collisional quenching. Lakowicz[19] derives the appropriate quadratic form shown in eq 2 that should fit the data.

$$\frac{I_0}{I} = (1 + K_D[Q])(1 + K_S[Q]) \qquad (2)$$

Yet, we have found very poor fits of our data using this approach.

In the remainder of this work, we posit a different situation, in which both types of quenching are occurring on the same

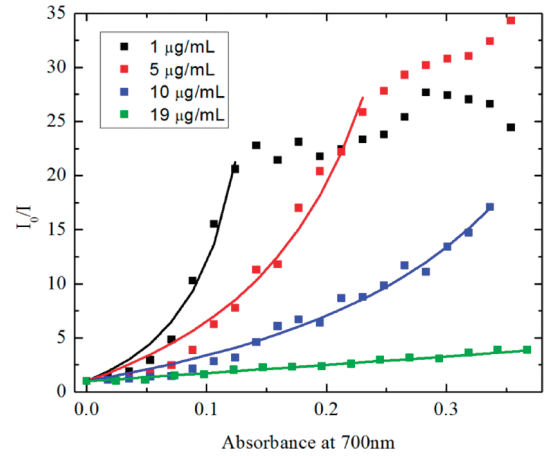

Figure 8. Stern−Volmer plots for MEH-PPV in DCB with various concentrations of SWCNT added as quencher, represented by absorbance at 700 nm. The solid squares represent actual data points, and the solid lines represent fits to the data using the model described in this work.

quencher. Driven by the relative strength of interaction between polymer and solvent and comparatively low rigidity, MEH-PPV and CN-PPV polymers are able to physically bind and thus coat the much larger SWCNTs in some part. The nanotube is then able to quench both polymers that have wrapped around it, along with additional unbound polymers through diffusional quenching. We continue to show the derivation and validity of a new model that describes our data well. We consider first the Stern−Volmer plots of MEH-PPV in DCB as a function of the MEH-PPV concentration. We consider the application of this model to MEH-PPV in DMA and then to CN-PPV in DMA and DCB.

A similar Stern−Volmer plot is shown in Figure 8 for the fluorescence quenching of MEHPPV by SWCNTs in DCB with a range of MEHPPV concentrations under study. An upwardly sigmoidal curvature is observed for each case, but the plateau is observed only for the two lowest concentrations of MEHPPV. Maximum amounts of quenching are therefore observed only at low concentrations of polymer: as the concentration of polymer increases, the extent of quenching is limited only by the concentration of quencher.

These trends depicted in Figure 8 are reproducible and the basis for the new model of binding between polymer chains and SWCNTs as presented below. The curvature is demonstrable in all of our Stern−Volmer type plots, and the saturation of fluorescence quenching at low concentrations of polymer is recurrent. The extent of curvature decreases quantifiably with increased polymer concentration, and the onset of the plateau, indicative of saturation, is proposed to signify a polymer-concentration dependent maximum of coverage of the SWCNTs present in solution.

A derivation and justification of our proposed model can be broken down into parts. First, the concentration of polymer *in solution* as a function of the SWCNT concentration will be given by the initial concentration minus the polymer that is bound to the SWCNT. The initial concentration (in the absence of SWCNTs) is denoted $C_{\text{initial,polymer}}$. We introduce a unitless constant associated with complexation, K_{static}, which is independent of the SWCNT concentration. This constant represents the concentration of MEH-PPV that will be bound per concentration (μg/mL) of SWCNT and, thus, is given as a weight percent ratio. We can now consider the equation that describes the unbound polymer concentration, UC_{polymer}, in solution as a

function of initial polymer concentration, and consistent with conservation of mass:

$$UC_{polymer} = C_{initial,polymer} - C_{SWCNT}K_{static} \quad (3)$$

Second, we start to consider the quenching itself. In a Stern−Volmer graph, we plot the ratio of fluorescence intensity with no quencher to fluorescence intensity as a function of quencher concentration. The intensity of fluorescence in the absence of quencher is proportional to the quantum yield of fluorescence of the polymer multiplied by the absorbance or optical density of the solution. The intensity of the fluorescence with quencher present is dominated by the fluorescence of any polymer still in solution, given that polymer bound to the SWCNT will in large part be quenched. Therefore the fluorescence as a function of quencher concentration is proportional to the quantum yield, Φ, of fluorescence of the polymer multiplied by the new absorbance or optical density of polymer remaining in solution. This line of reasoning is illustrated by eq 4. After cancellation of the quantum yield and proportionality constant, we obtain a relationship that describes the impact of static quenching.

$$\frac{I_0}{I} = \frac{k_{prop}\Phi_{fluor,polymer}C_{initial,polymer}}{k_{prop}\Phi_{fluor,polymer}(UC_{polymer})} = \frac{C_{initial,polymer}}{C_{initial,polymer} - C_{SWCNT}K_{static}} \quad (4)$$

Third, we start to consider the possibility of dynamic quenching of unbound polymer in solution. Because the possibility for additional bimolecular quenching is present if any areas of a SWCNT are exposed to collisions, the diffusional quenching constant must therefore vary on the basis of the extent of SWCNT wrapping the polymer can perform. We refer to the diffusional quenching constant as $K_{dynamic}$.

In general, the fractional fluorescence remaining, described indirectly by any Stern−Volmer plot, is given by $F/F_0 = I/I_0$. Hence, when there is only static quenching, the fraction that fluoresces is made up of the unbound fluorophores. We can describe the fraction *not* complexed as f,

$$f = \frac{C_{initial,polymer} - C_{SWCNT}K_{static}}{C_{initial,polymer}} = \frac{I}{I_0} \quad (5)$$

Because we posit that both types of quenching are occurring simultaneously for each quencher, the ratio of intensities, I/I_0, must be described using the product of both fractions: fluorophores that are unbound and fluorophores that are not dynamically quenched.

$$\frac{I}{I_0} = f\frac{\gamma}{\gamma + k_q C_{SWCNT}} = \left(\frac{C_{initial,polymer} - C_{SWCNT}K_{static}}{C_{initial,polymer}}\right) \times \left(\frac{\gamma}{\gamma + k_q C_{SWCNT}}\right) \quad (6)$$

where γ is the combined radiative and nonradiative rate constant for the fluorophore's spontaneous relaxation of the excited state (the rate of fluorescence decay) in the absence of quencher. The reciprocal of eq 6 is what we actually plot in our Stern−Volmer graph:

$$\frac{I_0}{I} = \left(\frac{C_{initial,polymer}}{C_{initial,polymer} - C_{SWCNT}K_{static}}\right)\left(\frac{\gamma + k_q C_{SWCNT}}{\gamma}\right) \quad (7)$$

$$\frac{I_0}{I} = \left(\frac{C_{initial,polymer}}{C_{initial,polymer} - C_{SWCNT}K_{static}}\right)(1 + K_{dynamic}C_{SWCNT}) \quad (8)$$

Given that $K_{dynamic} = k_q/\gamma$, we note that $K_{dynamic}$ is inversely proportional to the rate of fluorescence decay for a fluorophore or that it is proportional to the fluorescence decay time for that fluorophore. Hence, we might expect $K_{dynamic}$ to be larger for CN-PPV, whose decay time in solution is 0.9 ns,[24] than for MEH-PPV, whose decay time in solution is 0.33 ns.[25]

We have two goals in the remainder of this work: (1) to demonstrate the validity of this model in fitting data measured in our experiments and (2) to consider the implications of the data regarding the physical chemistry of these composites and the formation of their complexes. The results of all fits of MEH-PPV dilution series in DCB are shown in Figure 9.

We consider the reproducibility of the data and the quality of the fits to be good, given that dispersions of single-walled carbon nanotubes are fundamentally inhomogeneous in terms of (a) the different chiralities, propensity for different defects along the nanotubes, and the small concentration of chemical impurities that are undoubtedly found in these samples; and (b) the inevitable variation in the extent of debundling, even with a dispersion process that is well controlled.

Regarding the physical chemistry implied by these fits to our model, it is noted that the static quenching constant increases as a function of polymer concentration while the dynamic quenching constant decreases. We interpret these trends in the following way: (1) We postulate that as the polymer concentration increases, the equilibrium constant dictating wrapping of the nanotubes also increases. We also recognize that as polymer concentration increases, we approach the limiting solubility of the polymer in a given solvent. This may be related to the increasing extent of wrapping of the nanotubes as the polymer concentration increases, with the nanotubes providing a seed for polymer aggregation or agglomeration as the solubility of the polymer in that solvent is approached. (2) The dynamic quenching constant must decrease as polymer concentration increases because the availability of quenching sites on the nanotubes is decreasing as each becomes more wrapped by polymer. Therefore, at low polymer concentrations, the SWCNTs can collisionally quench more polymers but as the SWCNTs become completely wrapped at high polymer concentrations, they are no longer able to dynamically quench. We go on to look at similar cases first with MEH-PPV in DMA in Figure 10.

Again, we consider the reproducibility of the data and the quality of the fits to be good, given the fundamentally inhomogeneous nature of the SWCNT dispersions. The static quenching constant continues to increase as a function of polymer concentration and dramatically increases to $81 \pm 27\%$ at only 9 μg/mL. Because DMA is a much poorer solvent for MEHPPV, it actually plays an active role in increasing the propensity of complexation between SWCNT and MEHPPV. The enthalpy of mixing between polymer and solvent is more endothermic in DMA than DCB, which increases the amount of wrapping of the SWCNTs; the two enthalpy driven processes of polymer mixing in solvent and polymer wrapping the nanotubes are in competition, and by increasing the enthalpy

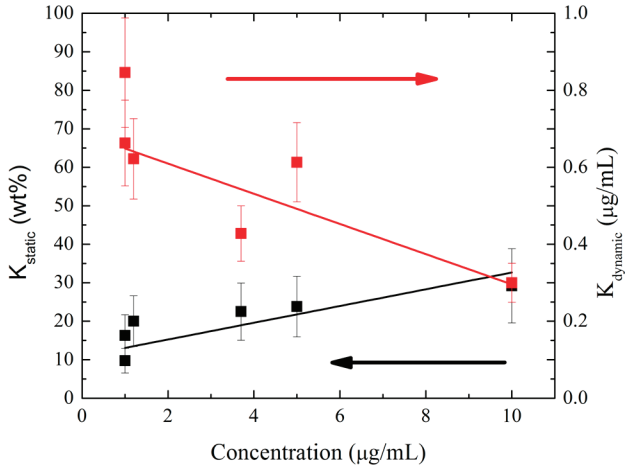

Figure 9. The set of fitting parameters for the derived model as applied to the fluorescence quenching data of MEH-PPV in DCB.

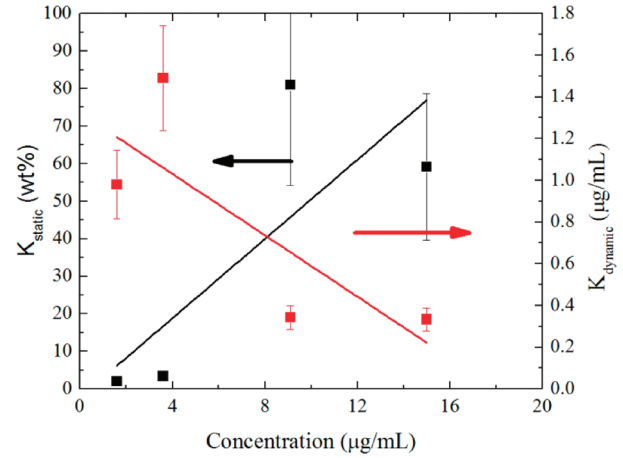

Figure 10. The set of fitting parameters for the derived model as applied to the fluorescence quenching data of MEH-PPV in DMA.

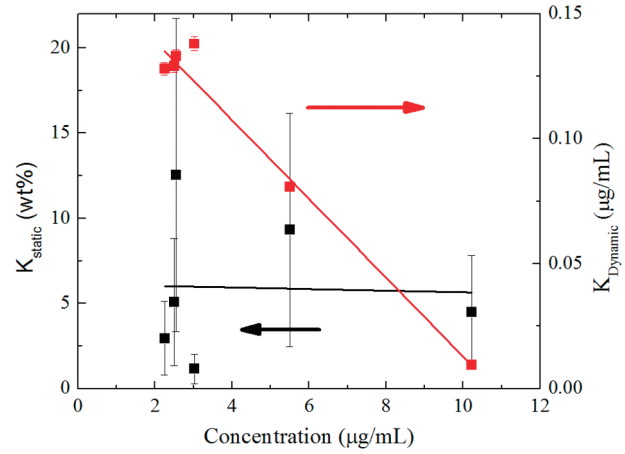

Figure 11. The set of fitting parameters for the derived model as applied to the fluorescence quenching data of CN-PPV in DCB.

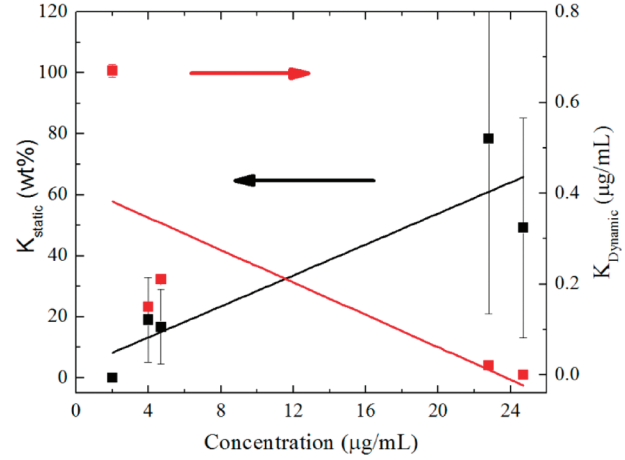

Figure 12. The set of fitting parameters for the derived model as applied to the fluorescence quenching data of CN-PPV in DMA.

of mixing polymer and solvent, we can in effect drive more polymers onto the SWCNTs.

The dynamic quenching constant generally decreases as the polymer concentration increases; it should also be higher in DMA than in DCB because the viscosity of the solvent is higher for DCB (1,2-DCB has a viscosity of 1.32×10^{-3} Pa s, and DMA has a viscosity of 0.92×10^{-3} Pa s at 20 °C; 1 cP = 1×10^{-3} Pa s). We expect the dynamic quenching constant to also be reflective of small changes in the fluorescence decay time as we change solvent. These expectations are consistent with the results in Figure 10.

We now go on to look at similar cases with CN-PPV in DCB and DMA. CN-PPV has a lower molecular weight than MEH-PPV, and hence, we expect solubilities might be higher because of a stronger entropy of mixing term. As a result, we expect that the static quenching constant will be smaller for the same micrograms per milliliter of polymer in solution when comparing with Figures 9 and 10. We also point out that CN-PPV is less sensitive to oxidative degradation. As a result, we do not expect to see the same extent of tetrahedral defects in the backbone that are believed to contribute to the formation of collapsed chains of MEH-PPV in solution.[26−29] We might expect CN-PPV to form more rigid extended chains in solution, regardless of the solvent quality. This is consistent with the observation that there is a negligible spectral shift shown in Figure 4b.

Again in Figures 11 and 12, we consider the reproducibility of the data and the quality of the fits to be good, given the fundamentally inhomogeneous nature of the SWCNT dispersions. We continue to observe the static quenching constant increasing as a function of the concentration of the polymer as a general trend. In agreement with our expectations that the static quenching constant will not be as high with CN-PPV for the same polymer concentration when compared with MEH-PPV, we see this term hit a maximum of 5−12% by weight at the polymer concentrations studied for CN-PPV in DCB as compared with 10−30% by weight for the concentrations of MEH-PPV in DCB that were studied. In addition, we see a similar trend with DMA as the solvent, as demonstrated by the fit lines.

We continue to see that the dynamic quenching constant decreases as the polymer concentration increases. Given that the static quenching constant does not rise rapidly, we can understand why the drop in dynamic quenching constant is small, although the trend downward is very clear. When we compare this with the case with MEH-PPV, we find that the dynamic quenching constant is typically smaller than for the same extent of nanotube-wrapping seen in Figures 9 and 10. This is unusual, given the longer excited state lifetime of the CN-PPV. It suggests that the extended conformation of the polymer plays a significant role in its diffusion to the nanotube and also in the necessary steric implications of subsequent interaction with the nanotube to allow effective quenching.

As we compare Figures 11 and 12, we can again make strong claims about the validity of our model because the dynamic

quenching constant remains reflective of changes in viscosity of the solvents. (1,2-DCB has viscosity of 1.32×10^{-3} Pa s, and DMA has viscosity of 0.92×10^{-3} Pa s at 20 °C; 1 cP = 1×10^{-3} Pa s). The generally larger dynamic quenching constants for DMA compared to DCB for the same weight percent coverage of nanotubes by the polymer supports this.

It is important to point out that despite the fact that concentration quenching occurs when polymers in solution are deposited to the solid state, we are neglecting this possible contribution to fluorescence quenching. For example, the quantum yields of MEH-PPV and CN-PPV will reduce from 0.35 in solution to 0.10 in the solid state and from 0.52 in solution to 0.35 in the solid state, respectively.[25] We choose to neglect this because while the polymer chains are becoming substantially closer to each other as a result of the wrapping process, in general, the nanotubes themselves are the most effective quencher overall; any excitation in a polymer chain bound to a metallic nanotube or semiconducing nanotube with appropriate LUMO level will be instantaneously quenched.

Conclusion

We have proposed and justified a model for the interaction of conjugated polymers and SWCNT based on the fluorescence quenching of the polymer by the nanotubes. The classical Stern−Volmer treatment of such fluorescence quenching is not valid for these macromolecules, but our model takes into account that both static quenching and dynamic quenching may occur on the same quencher, given its significant size in relation to the physical dimensions of the polymer chains.

We have shown the validity of our model by applying it to a multitude of solution series with two different conjugated polymers, MEH-PPV and CN-PPV in two different solvents, DMA and DCB, both of which are reasonable solvents for dispersing nanotubes. DMA is a poor solvent for the conjugated polymers,[18] and we recognize that the static quenching constant is a function of solvent quality for the polymer. This is because enhanced wrapping of the nanotube, interpreted from this data, occurs on account of the more endothermic enthalpy of mixing of the polymer and the solvent as solvent quality decreases.

We have qualitatively demonstrated the likely impact of solvent viscosity in the dynamic quenching of the polymers, consistent with typical predictions made and described by Lakowicz.[19]

Our results are far reaching for the following reasons. First, we have demonstrated a technique by which we can quantitatively describe the extent of coverage by a surfactant, given that the surfactant fluoresces. Therefore, the relative strength of the surfactant can be measured by comparing dispersion level improvement with the extent of nanotube coverage. Ultimately, the better the surfactant, the more nanotubes that can be manipulated and subsequently deposited through spin-casting, inkjet printing, or spray-coating processes. This becomes particularly important in such applications as replacing ITO as the transmissive conductive layer[30] for organic light emitting diodes and photovoltaic devices. Second, by changing the molecular weight of a given polymer or by changing the functional groups on polymers or even on smaller molecular materials, we can begin to understand and predict the chemical behavior of the nanotubes themselves, typically considered to be relatively inert. Third, the well-known theory of static and dynamic quenching described by the Stern−Volmer model has been extended toward these macromolecular chemical systems in which the possibility exists for multiple fluorophores to be complexed to the same quencher.

Acknowledgment. We gratefully acknowledge the Donors of the American Chemical Society Petroleum Research Fund for partial support of this research. We also thank the Rochester Institute of Technology for funding of this work through the Department of Chemistry Daniel Pasto Award and through the College of Science Summer Research program. We also thank Michael Schettini, Matthew Brister, Sidney Coombs, and Jessica Alexander for past contributions to our ongoing work with polymer/SWCNT interactions.

References and Notes

(1) Conturbia, G.; Vinhas, R. G.; Landers, R.; Valente, G. M. S.; Baranauskas, V.; Nogueira, A. F. *J. Nanosci. Nanotechnol.* **2009**, *9*, 5850.
(2) Previti, F.; Patane, S.; Allegrini, M. *Appl. Surf. Sci.* **2009**, *255*, 9877.
(3) Liu, L.; Stanchina, W. E.; Li, G. *Appl. Phys. Lett.* **2009**, *94*, 233309.
(4) Mallajosyula, A. T.; Iyer, S. S. K.; Mazhari, B. *Jpn. J. Appl. Phys.* **2009**, *48*, 011503.
(5) Hatton, R. A.; Blanchard, N. P.; Tan, L. W.; Latini, G.; Cacialli, F.; Silva, S. R. P. *Org. Electron.* **2009**, *10*, 388.
(6) Khatri, I.; Adhikari, S.; Aryal, H. R.; Soga, T.; Jimbo, T.; Umeno, M. *App. Phys. Lett.* **2009**, *94*, 093509.
(7) Kymakis, E.; Kornilios, N.; Koudoumas, E. *J. Phys. D: Appl. Phys.* **2008**, *41*, 165110.
(8) Kymakis, E.; Stratakis, E.; Koudoumas, E. *Thin Solid Films* **2007**, *515*, 8598.
(9) Li, C.; Chen, Y.; Wang, Y.; Iqbal, Z.; Chhowalla, M.; Mitra, S. *J. Mater. Chem.* **2007**, *17*, 2406.
(10) Brabec, C. J. *Sol. Energy Mater. Sol. Cells* **2004**, *83*, 273.
(11) Janssen, R. A. J.; Hummelen, J. C.; Sariciftci, N. S. *MRS Bull.* **2005**, *30*, 33, and references therein.
(12) Terrones, M. *Ann. Rev. Mater. Res.* **2003**, *33*, 419.
(13) Nakayama, K.; Asakura, Y.; Yokoyama, M. *Mol. Cryst. Liq. Cryst.* **2004**, *424*, 217.
(14) Landi, B. J.; Ruf, H. J.; Worman, J. J.; Raffaelle, R. P. *J. Phys. Chem. B* **2004**, *108*, 17089.
(15) Collison, C. J.; O'Donnell, M. J.; Alexander, J. L. *J. Phys. Chem. C* **2008**, *112*, 15144.
(16) Zhou, W.; Bai, X.; Wang, E.; Xie, S. *Adv. Mater.* **2009**, *21*, 4565.
(17) Landi, B. J.; Castro, S. L.; Ruf, H. J.; Evans, C. M.; Bailey, S. G.; Raffaelle, R. P. *Sol. Energy Mater. Sol. Cells* **2005**, *87*, 733.
(18) Collison, C. J.; Pellizzeri, S.; Ambrosio, F. *J. Phys. Chem. B* **2009**, *113*, 5809.
(19) Lakowizc, J. R. *Principles in Fluorescence Spectroscopy*, 2nd ed.; Springer: New York, 1999.
(20) Kubista, M.; Sjöback, R.; Eriksson, S.; Albinsson, B. *Analyst* **1994**, *119*, 417.
(21) Wu, C.; Peng, H.; Jiang, Y.; McNeill, J. *J. Phys. Chem. B* **2006**, *110*, 14148.
(22) Wu, C.; Szymanski, C.; McNeill, J. *Langmuir* **2006**, *22*, 2956.
(23) Wang, J.; Wang, D.; Moses, D.; Heeger, A. J. *J. Appl. Polym. Sci.* **2001**, *82*, 2553.
(24) Samuel, I. D. W.; Rumbles, G.; Collison, C. J.; Moratti, S. C.; Holmes, A. B. *Chem. Phys.* **1998**, *227*, 75.
(25) Samuel, I. D. W.; Rumbles, G.; Collison, C. J. *Phys. Rev. B* **1995**, *52*, R11573.
(26) Traiphol, R.; Sanguansat, P.; Srikhirin, T.; Kerdcharoen, T.; Osotchan, T. *Macromolecules.* **2006**, *39*, 1165.
(27) Padmanaban, G.; Ramakrishnan, S. *J. Phys. Chem. B* **2004**, *108*, 14933.
(28) Padmanaban, G.; Ramakrishnan, S. *J. Am. Chem. Soc.* **2000**, *122*, 2244.
(29) Hu, D.; Yu, J.; Padmanaban, G.; Ramakrishnan, S.; Barbara, P. F. *Nano Lett.* **2002**, *2*, 1121.
(30) Hellstrom, S. L.; Lee, H. W.; Bao, Z. *ACS Nano* **2009**, *3*, 1423.

JP104705Y